RSC Advances

PAPER

View Article Online
View Journal | View Issue

Cite this: RSC Adv., 2016, 6, 14027

Bis(perylene diimide) with DACH bridge as non-fullerene electron acceptor for organic solar cells†

Guangpeng Gao,‡[ab] Xiaolong Zhang,‡[cde] Dong Meng,[ab] Andong Zhang,[ab] Yanxia Liu,[e] Wei Jiang,*[a] Yanming Sun*[cd] and Zhaohui Wang[a]

Received 15th December 2015
Accepted 21st January 2016

DOI: 10.1039/c5ra26777c

www.rsc.org/advances

In this paper, we designed, synthesized, and characterized a set of non-fullerene small molecules based on bis(perylene diimide) with DACH bridge. Theoretical calculations make clear that the introduction of the DACH bridge into PPDI forms a U-shape framework, with pi–pi interactions between PDIs. We investigate the performances of non-fullerene solar cells comprising racemic and enantiomerically pure DACH-PPDIs as the electron acceptor and PTB7-Th as the electron donor. As a consequence, a power conversion efficiency (PCE) of 4.68% is achieved with inverted device architecture. Furthermore, the device behaviour, morphological feature and charge transport properties were also investigated. It is a potential way to design highly efficient non-fullerene organic solar cell by tuning the structure of PDI to reach highly efficient photovoltaic performances.

Introduction

The current decades have witnessed an increasing academic attention towards bulk heterojunction (BHJ) organic solar cells (OSCs) with power conversion efficiencies (PCEs) exceeding 10% for single-junction devices.[1–4] Great progress has been benefited from the advancement of novel materials, morphology controlling, and the development and optimization of device architectures.[5,6] Exploiting electron acceptors blended with various donor materials is of great concern for a further increase of efficiencies and future application.[7–15] To overcome the shortcomings like tedious purification, weak absorption in the visible region and less tunable electronic structure of the commonly used fullerene derivatives, non-fullerene acceptors are emerging as an alternative in BHJ devices with the increasing PCEs up to 7% recently.[16–18]

As one of the most promising frameworks used as electron acceptors in OSCs, perylene diimides (PDIs) are attracting much attention on account of their ease of synthesis, structural and functional tunability, and excellent electron affinities.[19–21] Especially, PDI-based photoactive materials can be effectively obtained by connecting the PDI subunits through bay-region with various linkers (side-by-side)[12,22–25] or *via* the imide position directly by a single bond (head-to-head).[26–29] The twisted structures resulting from this strategy can avoid the severe aggregation of PDI core and thus induce more favorable nanoscale interpenetrating networks when blended with donors.[18,23,24,30]

We have been focusing on the chemistry and functionality of π-expanded PDI systems both along the longitudinal and latitudinal directions.[31] According to the design concept based on twisted PDI structure, three kinds of bay-linked (singly, doubly and triply) PDI dimer series in side-by-side pattern were screened to produce totally different photovoltaic performances ascribable to the resulting different degrees of twisting and flexibility of molecular structures.[32] In combination with carefully selecting side chains, interfacial optimization and device engineering, the side-by-side molecule linked by a single bond with two neighboring units of about 70° angle (SDIPDI) manifested impressive PCE close to 6%, among the highest performances for the PDI based small molecules in single-junction cells.[33–36] On the other hand, another twisted PDI dimer (PPDI) in head-to-head mode, featuring a nonplanar molecular conformation with two PDI segments perpendicularly to each other, was designed with fine-tuned side chains (6-undecyl) to afford a PCE of 6.41%,[37] much higher than the previously reported efficiency of 3.2% by Narayan and co-workers using 8-pentadecyl as the side chains.[38]

In view of chiral molecules with specific functions efficiently utilizing in opto-electronic devices and enantioseletive recognition, *etc.*, to the best of our knowledge, rarely has such chiral

[a]Key Laboratory of Organic Solids, Beijing National Laboratory for Molecular Sciences, Institute of Chemistry, Chinese Academy of Sciences, Beijing 100190, P. R. China. E-mail: jiangwei@iccas.ac.cn

[b]University of Chinese Academy of Sciences, Beijing 100049, P. R. China

[c]Key Laboratory of Bio-Inspired Smart Interfacial Science and Technology of Ministry of Education, Beihang University, Beijing 100191, P. R. China. E-mail: sunym@buaa.edu.cn

[d]Heeger Beijing Research and Development Center, Beihang University, Beijing 100191, P. R. China

[e]College of Physics, Liaoning University, No. 66 Chongshan Zhong Road, Huanggu District, Shenyang, P. R. China

† Electronic supplementary information (ESI) available. See DOI: 10.1039/c5ra26777c

‡ These two authors contributed equally to this work.

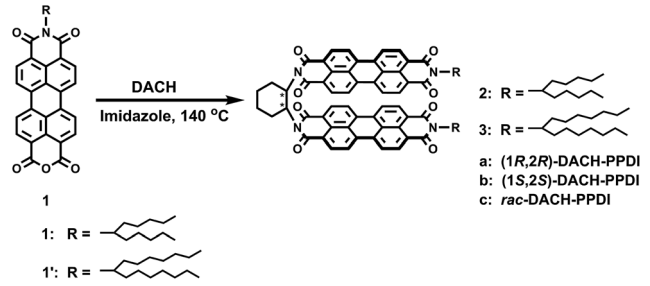

Scheme 1 Synthetic route to chiral bridged DACH-PPDIs.

molecule been determined to evaluate its efficiency as electron acceptor in OSCs to date.[39] These spur us to explore new non-fullerene materials with chirality as acceptors to compare the PCEs with their enantiomers. With this in mind, we have chosen racemic 1,2-diaminocyclohexane (*rac*-DACH) and enantiomerically pure 1*R*,2*R*-DACH and 1*S*,2*S*-DACH as bridges to develop chiral bridged PPDI derivatives, namely DACH-PPDIs (Scheme 1). The DACH subunit imparts chirality and C_2 symmetry onto the structure, also render a rigid scaffold with a very precisely defined disposition of the two amino groups.[40] The elaboration of chiral molecular clefts centered on the vicinal diamine group induce a kind of twisted structure with two PDI subunits form a U-shape framework according to the calculating result (Fig. S1c–f†). In this study, two branched alkyl chains have been introduced into the terminal amine sites with the aim of improving the solubility and molecular aggregation. In addition, a commercially available pseudo-2D donor polymer, namely poly[4,8-bis(5-(2-ethylhexyl)thiophen-2-yl)-benzo[1,2-*b*;4,5-*b*′]dithiophene-2,6-diyl-*alt*-(4-(2-ethylhexyl)-3-fluorothieno[3,4-*b*]thiophene-)-2-carboxylate-2-6-diyl] (PTB7-Th), was selected due to its high device efficiency when blending with various electron acceptors.[41,42] Both pure 1*R*,2*R*-enantiomers and 1*S*,2*S*-enantiomers as electron acceptors in the inverted architecture exhibit PCEs higher than 4.3% for DACH-PPDIs bearing 6-undecyl as the side chains, and a higher PCE of 4.68% was achieved for racemic DACH-PPDI (**2c**). This is first example reported to date for exploring chiral systems as electron acceptors in OSCs.

Experimental

Measurements and characterization

^{1}H NMR (400 MHz) and ^{13}C NMR (100 MHz) spectra were recorded in deuterated solvents on a Bruker ADVANCE 400 NMR spectrometer. *J* values are expressed in Hz and quoted chemical shifts are in ppm downfield from tetramethylsilane (TMS) reference using the residual protonated solvent as an internal standard. The signals have been designated as follows: s (singlet), d (doublet), t (triplet), q (quartet), dd (doublet of doublets), and m (multiplets). High resolution mass spectra (HRMS) were determined on IonSpec 4.7 Tesla Fourier Transform Mass Spectrometer.

UV-vis spectra were measured with Hitachi (Model U-3010) UV-vis spectrophotometer in a 1 cm quartz cell. Cyclic voltammograms (CVs) were recorded on a Zahner IM6e electrochemical workstation using glassy carbon discs as the working electrode, Pt wire as the counter electrode, Ag/AgCl electrode as the reference electrode at a scanning rate of 100 mV s^{-1} in film. 0.1 M tetrabutylammoniumhexafluorophosphate (Bu_4NPF_6) dissolved in CH_2Cl_2 or acetonitrile (HPLC grade) was employed as the supporting electrolyte, which was calibrated by the ferrocene/ferroncenium (Fc/Fc^+) as the redox couple. CH_2Cl_2 and acetonitrile were freshly distilled prior to use. Circular dichroism (CD) measurements were carried out on a Jasco-815 spectropolarimeter in a 1 cm path-length cell at room temperature. Spectra were collected with scan speed of 500 nm min^{-1} and response time of 0.5 s. Each spectrum was the average of three scans and corrected by chloroform. TGA measurements were performed on a PE TGA-7 instrument under a dry nitrogen flow, heating from room temperature to 550 °C, at a heating rate of 10 °C min^{-1}. Atomic force microscopy (AFM) images of blend films were obtained on a Multimode 8 Nanoscope V operating in the tapping mode. The films were made on Si wafer substrates under the best preparation conditions for solar cells.

Photovoltaic device fabrication and characterization

The solar cells were fabricated with an inverted structure of glass/ITO/ZnO/PTB7-Th : DACH-PPDIs/MoO_3/Al. Patterned ITO-coated substrates with a sheet resistance of ~15 ohm per square were cleaned using a detergent scrub and subsequently subjected to ultrasonic treatment in soap deionized water, deionized water, acetone and isopropyl alcohol for 15 minutes, separately. After drying overnight in an oven, the ITO substrates were treated with ultraviolet-ozone for 20 minutes, then ZnO precursor solution was spin-cast onto the ITO substrate at 4000 rpm for 20 s. ZnO film was heated at 230 °C for 15 min under ambient conditions. The substrates were transferred into an argon-filled glove box. A solution containing a mixture of PTB7-Th : DACH-PPDIs in *o*-dichlorobenzene at a concentration of PTB7-Th as 10 mg mL^{-1} was spin-cast for 60 s atop ZnO films with or without further annealing. Subsequently, MoO_3 (≈5 nm) and Al (≈100 nm) for the anode were deposited on the active layer under high vacuum. An active area of the devices was 10.0 mm^2, as measured from the geometrical overlap of the Al with the anode. During the measurement, an aperture with the area of 7.1 mm^2 was used to block stray light. Current density–voltage (*J*–*V*) characteristics were measured using a Keithley 2400 Source Measure Unit. Solar cell performance used an Air Mass 1.5 Global (AM 1.5 G) solar simulator (Class AAA solar simulator, Model 94063A, Oriel) with an irradiation intensity of 100 mW cm^{-2}, which was measured by a calibrated silicon solar cell and a readout meter (Model 91150V, Newport). EQE spectra were measured by using a QEX10 Solar Cell IPCE/Quantum Efficiency/Spectral Response measurement system (PV measurements, Inc.).

Carrier mobility

Carrier mobility was measured by space charge limit current (SCLC) method, where the electron mobility was measured with

the device structure of ITO/Al/PTB7-Th : DACH-PPDIs/Al and the hole mobility was measured with the device structure of ITO/MoO_3/PTB7-Th : DACH-PPDIs/MoO_3/Al. The mobility was determined by fitting the dark current to the model of a single carrier SCLC, described by the equation: $J = 9\varepsilon_0\varepsilon_r\mu_h(\mu_e)V^2/8d^3$, where J is the current density, ε_0 is the permittivity of free space, ε_r is the relative dielectric constant of the transport medium, μ_h is the hole mobility, μ_e is the electron mobility and d is the film thickness of the active layer. $V = V_{app} - V_{bi}$, where V_{app} is the applied voltage, V_{bi} is the offset voltage (V_{bi} is 0 V here). The carrier mobility was calculated from the slope of the $J^{1/2}$–V curves.

Materials

All chemicals, including *rac*-DACH and its optical pure 1*R*,2*R*- and 1*S*,2*S*-enantiomers, and solvents were purchased from commercial suppliers and used without further purification unless otherwise specified. *N*,*N*′-Bis(1-alkyl)perylene-3,4,9,10-tetracarboxylbisimide, *N*-(1-alkyl)perylene-3,4,9,10-tetracarboxyl-3,4-anhydride-9,10-imide was synthesized according to the literature.[43,44]

General synthetic procedure for chiral bridged PPDIs (2–3)

Perylene monoimide (PMI, **1**) (0.37 mmol), DACH (0.18 mmol) and imidazole (10 g) were added to a three-necked round bottom flask. The mixture was deoxygenated with argon for 5 min, then heated to 140 °C with vigorous stirring for 10 h. The cooled mixture was poured into water (200 mL), subsequently treated with 2 M HCl (50 mL) and stirred overnight. The resulting red solid was collected by vacuum filtration. The filter cake was washed neutral with distilled water, afterwards dried in vacuum at 60 °C. The solid was further purified by column chromatography on silica gel to afford **2** and **3** as red solids.

2a–2c. (Yields: 28%) eluted with CH_2Cl_2/MeOH (100 : 1).

2a: ^{1}H NMR (400 MHz, $CDCl_3$): δ = 8.67 (d, J = 7.9 Hz, 2H), 8.57–8.48 (m, 10H), 8.41 (dd, J = 13.4, 8.1 Hz, 4H), 6.42–6.40 (m, 2H), 5.15–5.08 (m, 2H), 2.77–2.75 (m, 2H), 2.19–2.16 (m, 4H), 2.06–1.98 (m, 4H), 1.83–1.74 (m, 6H), 1.25–1.23 (m, 24H), 0.79 (t, J = 6.6 Hz, 12H). ^{13}C NMR (100 MHz, $CDCl_3$): δ = 163.71, 163.60, 134.18, 134.13, 131.51, 131.25, 129.32, 129.27, 126.13, 126.05, 123.88, 122.99, 122.82, 122.75, 122.69, 122.55, 54.72, 53.31, 32.24, 31.70, 29.71, 29.25, 26.61, 25.62, 22.52, 14.00. HRMS (MALDI(N), 100%): calcd (%) for $C_{76}H_{72}N_4O_8$: 1168.53556; found, 1168.53588.

2b: ^{1}H NMR (400 MHz, $CDCl_3$): δ = 8.68 (d, J = 8.0 Hz, 2H), 8.58–8.49 (m, 10H), 8.42 (dd, J = 12.9, 8.1 Hz, 4H), 6.42–6.40 (m, 2H), 5.16–5.09 (m, 2H), 2.77–2.75 (m, 2H), 2.22–2.17 (m, 4H), 2.06–1.98 (m, 4H), 1.84–1.74 (m, 6H), 1.26–1.23 (m, 24H), 0.79 (t, J = 6.6 Hz, 12H). ^{13}C NMR (100 MHz, $CDCl_3$): δ = 163.68, 163.53, 134.07, 134.03, 131.38, 131.17, 129.24, 129.21, 126.03, 125.96, 123.88, 122.98, 122.74, 122.67, 122.61, 122.44, 54.71, 53.26, 32.22, 31.69, 29.20, 26.62, 25.61, 22.52, 13.99. HRMS (MALDI(N), 100%): calcd (%) for $C_{76}H_{72}N_4O_8$: 1168.53556; found, 1168.53584.

2c: ^{1}H NMR (400 MHz, $CDCl_3$): δ = 8.68 (d, J = 8.0 Hz, 2H), 8.59–8.50 (m, 10H), 8.43 (dd, J = 12.3, 8.2 Hz, 4H), 6.42–6.40 (m, 2H), 5.16–5.09 (m, 2H), 2.77–2.74 (m, 2H), 2.23–2.15 (m, 4H), 2.07–1.98 (m, 4H), 1.84–1.72 (m, 6H), 1.23 (m, 24H), 0.79 (t, J = 6.6 Hz, 12H). ^{13}C NMR (100 MHz, $CDCl_3$): δ = 163.68, 163.60, 134.20, 134.14, 131.55, 131.24, 129.34, 129.26, 126.14, 126.07, 123.86, 122.98, 122.82, 122.75, 122.71, 122.59, 54.72, 53.38, 32.25, 31.70, 29.31, 26.61, 25.64, 22.52, 14.00. HRMS (MALDI(N), 100%): calcd (%) for $C_{76}H_{72}N_4O_8$: 1168.53556; found, 1168.53576.

3a–3c. (Yields: 43%) eluted with CH_2Cl_2.

3a: ^{1}H NMR (400 MHz, $CDCl_3$): δ = 8.67 (d, J = 8.0 Hz, 2H), 8.57–8.48 (m, 10H), 8.41 (dd, J = 13.6, 8.1 Hz, 4H), 6.42–6.40 (m, 2H), 5.15–5.08 (m, 2H), 2.77–2.75 (m, 2H), 2.22–2.16 (m, 4H), 2.06–1.98 (m, 4H), 1.83–1.74 (m, 6H), 1.26–1.17 (m, 40H), 0.78–0.77 (m, 12H). ^{13}C NMR (100 MHz, $CDCl_3$): δ = 163.65, 163.47, 134.01, 131.30, 131.12, 129.20, 129.15, 125.97, 125.90, 123.87, 122.94, 122.69, 122.62, 122.38, 54.73, 53.23, 32.27, 31.76, 29.46, 29.18, 26.98, 25.60, 22.56, 14.01. HRMS (MALDI(N), 100%): calcd (%) for $C_{84}H_{88}N_4O_8$: 1280.66076; found, 1280.66051.

3b: ^{1}H NMR (400 MHz, $CDCl_3$): δ = 8.67 (d, J = 8.0 Hz, 2H), 8.57–8.48 (m, 10H), 8.41 (dd, J = 13.4, 8.4 Hz, 4H), 6.42–6.37 (m, 2H), 5.16–5.08 (m, 2H), 2.77–2.75 (m, 2H), 2.22–2.14 (m, 4H), 2.06–1.98 (m, 4H), 1.84–1.71 (m, 6H), 1.26–1.17 (m, 40H), 0.80–0.77 (m, 12H). ^{13}C NMR (100 MHz, $CDCl_3$): δ = 163.68, 163.55, 134.14, 134.10, 131.45, 131.21, 129.30, 129.24, 126.09, 126.02, 123.89, 122.98, 122.78, 122.71, 122.65, 122.50, 54.74, 53.29, 32.30, 31.76, 29.46, 29.18, 26.97, 25.62, 22.56, 14.01. HRMS (MALDI(N), 100%): calcd (%) for $C_{84}H_{88}N_4O_8$: 1280.66076; found, 1280.66029.

3c: ^{1}H NMR (400 MHz, $CDCl_3$): δ = 8.67 (d, J = 8.0 Hz, 2H), 8.57–8.49 (m, 10H), 8.42 (dd, J = 12.8, 8.2 Hz, 4H), 6.42–6.40 (m, 2H), 5.16–5.08 (m, 2H), 2.77–2.74 (m, 2H), 2.22–2.14 (m, 4H), 2.06–1.98 (m, 4H), 1.84–1.72 (m, 6H), 1.26–1.17 (m, 40H), 0.79–0.77 (m, 12H). ^{13}C NMR (100 MHz, $CDCl_3$): δ = 163.65, 163.56, 134.14, 131.49, 131.19, 129.31, 129.24, 126.11, 126.03, 123.87, 122.98, 122.77, 122.67, 122.54, 54.74, 53.38, 32.30, 31.76, 29.47, 29.31, 29.18, 26.97, 25.65, 22.56, 14.01. HRMS (MALDI(N), 100%): calcd (%) for $C_{84}H_{88}N_4O_8$: 1280.66076; found, 1280.66102.

Results and discussion

Synthesis

Compounds DACH-PPDIs (**2** and **3**) were synthesized in moderate yields *via* amidation between perylene monoimide (PMI, **1** and **1′**) with DACH, shown in Scheme 1. Besides racemic DACH, 1*R*,2*R*-enantiomer and 1*S*,2*S*-enantiomer are available, so the enantiomerically pure and racemic products for compounds **2** and **3** are achieved for fully exploring the influence of different configuration on the device efficiencies. The products were fully characterized by ^{1}H NMR and ^{13}C NMR, and high resolution mass spectroscopy (HRMS). These compounds are readily soluble in common organic solvents such as dichloromethane (DCM) and dichlorobenzene (DCB) at room temperature for solubilizing alkyl substituents.

Theoretical calculations

Theoretical calculations were performed using density functional theory (DFT) with Gaussian 09 program, D.01 Revision.[45]

Considering that the non-covalent interaction between two PDI planes may have an influence on the geometry, two functionals including dispersion, ωB97XD and APFD, were used to optimize the geometry of DACH-PPDI with the basis set 6-31g(d).[46–48] The two methods give the similar results and give a good understanding of the geometric construction of DACH-PPDI. As shown in Fig. S1c and d,† referable to the split between vicinal diamine groups, the planes of PDIs are irregular and face to face closely, the two pieces of PDIs stagger slightly from each other to form a deflective angle as 17.70°, the angle of the two planes is about 1.62°, nearly parallel to each other, the distance of the centroids of the two planes is about 3.45 Å. As to APFD (Fig. S1e and f†), the deflective angle of the two pieces of PDIs is about 16.61°, the angle of the two planes is about 1.68° and the distance of the centroids of the two planes is about 3.34 Å. The introduction of the DACH bridge into PPDI forms a U-shape framework with pi–pi interactions between PDIs and demonstrates a more twisted molecular configuration.

Optical, electrochemical and thermal properties

These bridged PPDIs **2** and **3** reveal similar and strong absorption bands in the range of 450–550 nm assigned as perylene core with high molar extinction coefficient of larger than 10^5 M^{-1} cm^{-1} in chloroform solution (10^{-5} M) (Fig. S2a and Table S1†). The introduction of different branched alkyl chains has no obvious influence on the longest absorption maxima and only slight changes in absorptivity. The bridge induces similar bands in the near UV region which can contribute to light harvesting of solar devices. Be confronted with the absorption in solution, the thin films present a similar but broader absorption (Fig. S2b–g†). At the same time, slight redshifts of about 8–10 nm for all compounds have been observed in films compared to those in solution, which indicates that there are weak intermolecular interactions and molecular aggregation in the film. Calculated from the absorption edges in solution, their corresponding optical band gaps are approximately 2.28 eV. The normalized UV-vis absorption spectra of **2c**, PTB7-Th, and their 1 : 2 ratio of blends in film are displayed in Fig. 1, from which we can see a complementary absorption of PTB7-Th during 500 nm to 800 nm. As for the absorption of the PTB7-Th : **2c** blend film, a wide absorption covering almost the whole visible range from 400 nm to 800 nm is observed. Anatomizing this characteristic, we can affirm that the active layer could absorb as many photons as possible, which have a big contribution to a better short circuit-current density (J_{SC}) of the photovoltaic device.

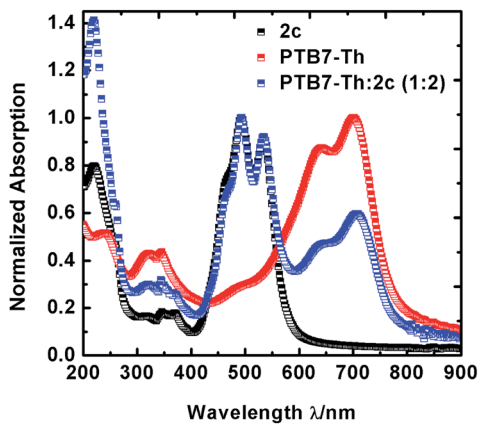

Fig. 1 Normalized UV-vis absorption spectra of **2c**, PTB7-Th, and 1 : 2 ratio of PTB7-Th : **2c** films.

Electrochemical cyclic voltammetry (CV) was used to investigate the energy levels of these bridged PPDIs (Fig. S3†), all of which show two reversible reduction waves. The lowest unoccupied molecular orbital energy levels (LUMOs) were determined to be −3.88 eV for both **2** and **3**, which are almost the same as that of PPDI.[29] Consequently, the highest occupied molecular orbital energy levels (HOMOs) were estimated to be about −6.16 eV for both **2** and **3**, which are *ca.* 0.26 eV lower in comparison with that of PPDI (−5.90 eV)[29] attributing to the donating effect of bridges (Table S1†). The energy level diagrams of DACH-PPDIs and PTB7-Th are illustrated in Fig. S4a.† The energy offset between the HOMO of PTB7-Th (−5.22 eV)[37] and the LUMO of DACH-PPDIs is 1.34 eV, thus, a high V_{OC} is anticipated.

The thermal properties of these bridged PPDIs were investigated by thermo gravimetric analysis (TGA) under nitrogen as portrayed in Fig. S5 and Table S1.† From the TGA graph, it can be seen that they possess excellent thermal stability with decomposition temperature of 5% weight loss over 390 °C. Furthermore, the absolute configurations of these PPDI enantiomers were clearly evaluated by their CD spectra (Fig. S6†). As the enantiomers of **2a**, **2b**, **3a** and **3b** having C_2 symmetric axis, the CD spectra of them in chloroform solution (10^{-5} M) revealed perfect mirror images.

Photovoltaic performances

In order to explore the potential application of bridged PPDIs as an electron acceptor in BHJ organic solar cells, the inverted device architecture of ITO/ZnO/PTB7-Th : DACH-PPDIs/MoO_3 (5 nm)/Al (100 nm) has been studied in this work (Fig. S4b†). A sol–gel-derived ZnO was used as the electron transport layer, and evaporated MoO_3 was used as the hole transport layer. Comparing with conventional structure, using ZnO as electron transport layer with highly transparent feature could decrease optical loss. Fig. S4a† shows that the offset of LUMO energy levels of donor and acceptor is about 0.24 eV, which forms electric field enough to separate exciton that are generated by donor in the bulk heterojunction. The value of valence band of MoO_3 is close to HOMO of PTB7-Th, which facilitates the transfer of holes to electrode and reduction of the energy loss. The device parameters of V_{OC}, short circuit current (J_{SC}), fill factor (FF), and PCE are summarized in Table S3,† while current density–voltage (J–V) characteristics are revealed in Fig. 2a and S8.†

We firstly scanned the different D/A ratios with different rotating speeds under the annealing temperature of 70 °C, the PCEs raised along with the D/A ratios changing from 1 : 1 to 1 : 2, but decreased when D/A ratio was 1 : 2.5. The optimized ratio as 1 : 2 for all devices are summarized in Table 1. Then, we examined the influences of thermal annealing temperature on

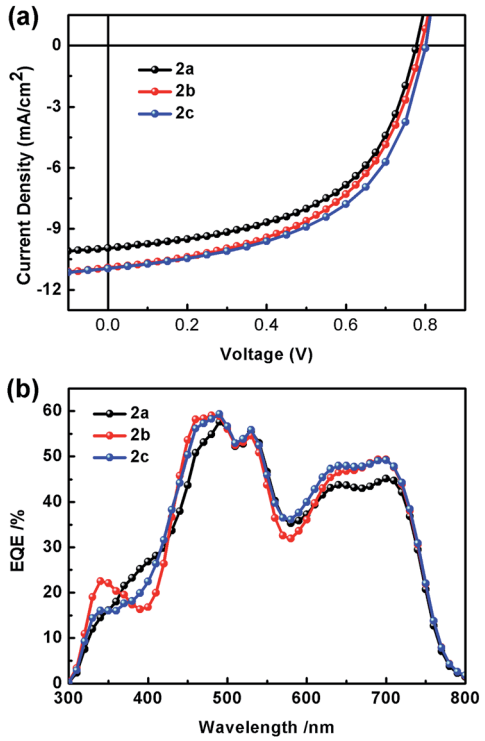

Fig. 2 (a) *J*–*V* and (b) EQE curves of the OSCs based on PTB7-Th : DACH-PPDIs (**2a–2c**) combinations (1 : 2 ratio, w/w).

the device performances based on PTB7-Th : **2c**. Remarkable PCE of 4.68% have been obtained when the annealing temperature is 70 °C, with a J_{SC} of 10.96 mA cm^{-2}, a V_{OC} of 0.80 V, and an FF of 53.30%. But the PCE decreased to 3.48% while further elevating the annealing temperature to 90 °C and just reached to 3.00% without annealing (Table S2†). Under the annealing temperature of 70 °C, the PCEs of pure 1*R*,2*R*-, and 1*S*,2*S*-enantiomers of **2a** and **2b** can reach 4.36% and 4.42%, respectively, which are a little lower than the PEC of **2c**. The outcome probably due to the better miscibility between the racemic **2c** with donor polymer. To study the effect of different terminal chains, 8-pentadecyl analogues with a longer tail were also used as acceptors. After extending the side chains from 6-undecyl to 8-pentadecyl, situation was getting worse, rather than better. Though exhibiting better photovoltaic performances compared to the pure enantiomers **3a** and **3b**, the PCE of racemic **3c** dropped a bit to 3.97% in comparison with **2c**, which presumably imputable to weak molecular aggregation between donor polymer and 8-pentadecyl-DACH-PPDIs (Fig. S9†).

As displayed in Fig. 2b, the external quantum efficiency (EQE) spectra of the non-fullerene OSC devices employing PTB7-Th with different acceptor blends (**2a–2c**) depicted a much broad photoresponse ranging from 300 to 800 nm. The photo response ranging from 400–570 nm attributed to the absorption of acceptors, which is a little higher than the absorption of PTB7-Th in the range of 570–800 nm. The broadband spectra indicate that both polymer donors and non-fullerene acceptors contribute to the generation of excitons in devices. Impressively, the top-performing PTB7-Th : DACH-PPDIs devices reach the highest EQE value of 60% at 490 nm, which is among the highest values reported so far.

Morphological properties and charge transport properties

To probe the topography and phase morphologies of the blend films based on PTB7-Th : DACH-PPDIs non-fullerene systems, atomic force microscopy (AFM) in a tapping mode were taken directly from the best photovoltaic devices as shown in Fig. S7.† The blend films display smooth and uniform surface morphology. It can be observed that PTB7-Th : DACH-PPDIs blend films exhibited a low root-mean-square roughness (RMS) of 0.61–0.70 nm but had similar AFM images with no evidence of large scale segregation. This suggests that all acceptors phase separate on a similar scale with PTB7-Th arise from the resemblance between **2** and **3**.

Space charge limited current (SCLC) was used to probe the carrier transport properties by measuring the hole and electron mobility of PTB7-Th : DACH-PPDIs blend films, the results are presented in Table 2 and S10.† As shown in Table 2, all the blend

Table 2 Hole and electron mobilities of PTB7-Th/DACH-PPDIs blend films

Blends	μ_e cm^2 V^{-1} s^{-1}	μ_h cm^2 V^{-1} s^{-1}	μ_h/μ_e ratio
PTB7-Th : **2a**	7.98×10^{-4}	1.35×10^{-3}	1.70
PTB7-Th : **2b**	8.04×10^{-4}	9.11×10^{-4}	1.13
PTB7-Th : **2c**	8.38×10^{-4}	9.71×10^{-4}	1.16
PTB7-Th : **3a**	8.34×10^{-4}	8.67×10^{-4}	1.04
PTB7-Th : **3b**	9.06×10^{-4}	9.79×10^{-4}	1.08
PTB7-Th : **3c**	8.71×10^{-4}	9.41×10^{-4}	1.08

Table 1 Photovoltaic parameters of the OSCs with an inverted structure based on PTB7-Th : DACH-PPDIs **2** and **3** (1 : 2, w/w), under the annealing temperature of 70 °C

Acceptor	V_{OC} [V]	J_{SC} [mA cm^{-2}]	FF [%]	PCE[a] [%]
2a	0.77 ± 0.006	10.52 ± 0.37	50.40 ± 1.63	4.09 ± 0.15 (4.36)
2b	0.79 ± 0.003	10.47 ± 0.34	51.47 ± 0.56	4.25 ± 0.11 (4.42)
2c	0.80 ± 0.006	10.63 ± 0.39	51.40 ± 1.56	4.34 ± 0.20 (4.68)
3a	0.79 ± 0.010	9.56 ± 0.33	50.03 ± 1.12	3.78 ± 0.05 (3.87)
3b	0.80 ± 0.006	9.51 ± 0.15	49.78 ± 1.15	3.80 ± 0.06 (3.85)
3c	0.81 ± 0.007	9.55 ± 0.23	50.55 ± 1.47	3.90 ± 0.06 (3.97)

[a] Tested under the illumination of AM 1.5 G 100 mW cm^{-2}. The values in parentheses refer to the max PCEs obtained from over five devices.

films exhibited higher μ_e and μ_h, and the blend films of **2c** under the optimal conditions has a electron mobility (μ_e) of 8.38×10^{-4} cm^2 V^{-1} s^{-1} and hole mobility (μ_h) of 9.71×10^{-4} cm^2 V^{-1} s^{-1}, corresponding to nearly balanced charge transport ($\mu_h/\mu_e = 1.16$). The results indicated that both hole and electron mobility are not the limiting factor for achieving high J_{SC} and FF.

Conclusions

In conclusion, a set of molecules based on PPDIs with a chiral and twisted bridge were designed, synthesized and characterized for non-fullerene acceptors in OSCs. A broad and strong absorption band in the visible region, and a proper energy offset (1.34 eV) in BHJ blend films were achieved for solar cells fabricated with these chiral bridged PPDIs as the electron acceptor and PTB7-Th as the electron donor. The racemic mixture of both 6-undecyl and 8-pentadecyl substituted compounds exposed a little higher PCEs than those of their pure 1*R*,2*R*-enantiomers and 1*S*,2*S*-enantiomers, probably due to the better miscibility between the raceme with donor polymer than the pure enantiomers. In addition, the indications that OSC devices of **2** universally reveal higher photovoltaic performances than **3** demonstrate that DACH-PPDIs with 6-undecyl match better with PTB7-Th. As a result, a very promising PCE of 4.68% was achieved in the PTB7-Th : **2c** BHJ devices. Chemical fabrication of PBI-based chiral materials has certain guiding significance for the improvement of PCEs in non-fullerene BHJ organic solar cells.

Acknowledgements

For financial support of this research, we thank 973 Program (Grant 2014CB643502 and 2012CB932903), the National Natural Science Foundation of China (21225209, 21190032, and 51473009), NSFC-DFG Joint Project TRR61, and the Chinese Academy of Sciences.

Notes and references

1 Y. H. Liu, J. B. Zhao, Z. K. Li, C. Mu, W. Ma, H. W. Hu, K. Jiang, H. R. Lin, H. Ade and H. Yan, *Nat. Commun.*, 2014, **5**, 5293.
2 J. B. You, L. T. Dou, K. Yoshimura, T. Kato, K. Ohya, T. Moriarty, K. Emery, C. C. Chen, J. Gao, G. Li and Y. Yang, *Nat. Commun.*, 2013, **4**, 1446.
3 A. R. b. M. Yusoff, D. Kim, H. P. Kim, F. K. Shneider, W. J. da Silva and J. Jang, *Energy Environ. Sci.*, 2015, **8**, 303–316.
4 Z. Zheng, S. Q. Zhang, M. J. Zhang, K. Zhao, L. Ye, Y. Chen, B. Yang and J. H. Hou, *Adv. Mater.*, 2015, **27**, 1189–1194.
5 A. W. Hains, Z. Q. Liang, M. A. Woodhouse and B. A. Gregg, *Chem. Rev.*, 2010, **110**, 6689–6735.
6 Y. Huang, E. J. Kramer, A. J. Heeger and G. C. Bazan, *Chem. Rev.*, 2014, **114**, 7006–7043.
7 C. B. Nielsen, S. Holliday, H. Y. Chen, S. J. Cryer and I. McCulloch, *Acc. Chem. Res.*, 2015, **48**, 2803–2812.
8 A. F. Eftaiha, J. P. Sun, I. G. Hill and G. C. Welch, *J. Mater. Chem. A*, 2014, **2**, 1201–1213.
9 Z. H. Lu, B. Jiang, X. Zhang, A. L. Tang, L. L. Chen, C. L. Zhan and J. N. Yao, *Chem. Mater.*, 2014, **26**, 2907–2914.
10 H. R. Lin, S. S. Chen, Z. K. Li, J. Y. L. Lai, G. F. Yang, T. McAfee, K. Jiang, Y. K. Li, Y. H. Liu, H. W. Hu, J. B. Zhao, W. Ma, H. Ade and H. Yan, *Adv. Mater.*, 2015, **27**, 7299–7304.
11 Y. Z. Lin and X. W. Zhan, *Mater. Horiz.*, 2014, **1**, 470–488.
12 W. Ni, M. M. Li, F. Liu, X. J. Wan, H. R. Feng, B. Kan, Q. Zhang, H. T. Zhang and Y. S. Chen, *Chem. Mater.*, 2015, **27**, 6077–6084.
13 Y. M. Sun, J. Seifter, L. J. Huo, Y. L. Yang, B. B. Y. Hsu, H. Q. Zhou, X. B. Sun, S. Xiao, L. Jiang and A. J. Heeger, *Adv. Energy Mater.*, 2015, **5**, 1400987.
14 A. Najari, S. Beaupré, N. Allard, M. Ouattara, J. R. Pouliot, P. Charest, S. Besner, M. Simoneau and M. Leclerc, *Adv. Energy Mater.*, 2015, **5**, 1501213.
15 K. Cnops, B. P. Rand, D. Cheyns, B. Verreet, M. A. Empl and P. Heremans, *Nat. Commun.*, 2014, **5**, 3406.
16 D. Sun, D. Meng, Y. H. Cai, B. B. Fan, Y. Li, W. Jiang, L. J. Huo, Y. M. Sun and Z. H. Wang, *J. Am. Chem. Soc.*, 2015, **137**, 11156–11162.
17 Y. Zhong, M. T. Trinh, R. S. Chen, G. E. Purdum, P. P. Khlyabich, M. Sezen, S. Oh, H. M. Zhu, B. Fowler, B. Y. Zhang, W. Wang, C. Y. Nam, M. Y. Sfeir, C. T. Black, M. L. Steigerwald, Y. L. Loo, F. Ng, X. Y. Zhu and C. Nuckolls, *Nat. Commun.*, 2015, **6**, 8242.
18 Y. J. Hwang, H. Y. Li, B. A. E. Courtright, S. Subramaniyan and S. A. Jenekhe, *Adv. Mater.*, 2016, **28**, 124–131.
19 C. Li and H. Wonneberger, *Adv. Mater.*, 2012, **24**, 613–636.
20 F. Würthner and M. Stolte, *Chem. Commun.*, 2011, **47**, 5109–5115.
21 Y. Avlasevich, C. Li and K. Müllen, *J. Mater. Chem.*, 2010, **20**, 3814–3826.
22 Q. F. Yan, Y. Zhou, Y. Q. Zheng, J. Pei and D. H. Zhao, *Chem. Sci.*, 2013, **4**, 4389–4394.
23 Y. H. Liu, J. Y. L. Lai, S. S. Chen, Y. K. Li, K. Jiang, J. B. Zhao, Z. K. Li, H. W. Hu, T. X. Ma, H. R. Lin, J. Liu, J. Zhang, F. Huang, D. M. Yu and H. Yan, *J. Mater. Chem. A*, 2015, **3**, 13632–13636.
24 Y. H. Liu, C. Mu, K. Jiang, J. B. Zhao, Y. K. Li, L. Zhang, Z. K. Li, J. Y. L. Lai, H. W. Hu, T. X. Ma, R. R. Hu, D. M. Yu, X. H. Huang, B. Z. Tang and H. Yan, *Adv. Mater.*, 2015, **27**, 1015–1020.
25 Y. Z. Lin, Y. F. Wang, J. Y. Wang, J. H. Hou, Y. F. Li, D. B. Zhu and X. W. Zhan, *Adv. Mater.*, 2014, **26**, 5137–5142.
26 S. Rajaram, R. Shivanna, S. K. Kandappa and K. S. Narayan, *J. Phys. Chem. Lett.*, 2012, **3**, 2405–2408.
27 W. Q. Chen, X. Yang, G. K. Long, X. J. Wan, Y. S. Chen and Q. C. Zhang, *J. Mater. Chem. C*, 2015, **3**, 4698–4705.
28 Y. N. Du, L. L. Jiang, J. Zhou, G. J. Qi, X. Y. Li and Y. Q. Yang, *Org. Lett.*, 2012, **14**, 3052–3055.
29 L. Ye, K. Sun, W. Jiang, S. Q. Zhang, W. C. Zhao, H. F. Yao, Z. H. Wang and J. H. Hou, *ACS Appl. Mater. Interfaces*, 2015, **7**, 9274–9280.
30 Y. H. Cai, L. J. Huo, X. B. Sun, D. H. Wei, M. S. Tang and Y. M. Sun, *Adv. Energy Mater.*, 2015, **5**, 1500032.

31 W. Jiang, Y. Li and Z. H. Wang, *Acc. Chem. Res.*, 2014, **47**, 3135–3147.
32 W. Jiang, L. Ye, X. G. Li, C. Y. Xiao, F. Tan, W. C. Zhao, J. H. Hou and Z. H. Wang, *Chem. Commun.*, 2014, **50**, 1024–1026.
33 L. Ye, W. Jiang, W. C. Zhao, S. Q. Zhang, D. P. Qian, Z. H. Wang and J. H. Hou, *Small*, 2014, **10**, 4658–4663.
34 L. Ye, W. Jiang, W. C. Zhao, S. Q. Zhang, Y. Cui, Z. H. Wang and J. H. Hou, *Org. Electron.*, 2015, **17**, 295–303.
35 Y. Y. Fu, Q. Q. Yang, Y. F. Deng, W. Jiang, Z. H. Wang, Y. H. Geng and Z. Y. Xie, *Org. Electron.*, 2015, **18**, 24–31.
36 Y. Zang, C.-Z. Li, C.-C. Chueh, S. T. Williams, W. Jiang, Z.-H. Wang, J.-S. Yu and A. K.-Y. Jen, *Adv. Mater.*, 2014, **26**, 5708–5714.
37 C.-H. Wu, C.-C. Chueh, Y.-Y. Xi, H.-L. Zhong, G.-P. Gao, Z.-H. Wang, L. D. Pozzo, T.-C. Wen and A. K.-Y. Jen, *Adv. Funct. Mater.*, 2015, **25**, 5326–5332.
38 R. Shivanna, S. Shoaee, S. Dimitrov, S. K. Kandappa, S. Rajaram, J. R. Durrant and K. S. Narayan, *Energy Environ. Sci.*, 2014, **7**, 435–441.
39 A. Iwan, B. Boharewicz, I. Tazbir, V. Hamplová and A. Bubnov, *Solid-State Electron.*, 2015, **104**, 53–60.
40 T. P. Quinn, P. D. Atwood, J. M. Tanski, T. F. Moore and J. F. Folmer-Andersen, *J. Org. Chem.*, 2011, **76**, 10020–10030.
41 I. H. Jung, D. L. Zhao, J. Jang, W. Chen, E. S. Landry, L. Y. Lu, D. V. Talapin and L. P. Yu, *Chem. Mater.*, 2015, **27**, 5941–5948.
42 J. Q. Zhang, Y. J. Zhang, J. Fang, K. Lu, Z. Y. Wang, W. Ma and Z. X. Wei, *J. Am. Chem. Soc.*, 2015, **137**, 8176–8183.
43 Y. W. Huang, J. C. Hu, W. F. Kuang, Z. X. Wei and C. F. J. Faul, *Chem. Commun.*, 2011, **47**, 5554–5556.
44 R. C. Liu, M. W. Holman, L. Zang and D. M. Adams, *J. Phys. Chem. A*, 2003, **107**, 6522–6526.
45 M. J. Frisch, G. W. Trucks, H. B. Schlegel, G. E. Scuseria, M. A. Robb, J. R. Cheeseman, G. Scalmani, V. Barone, B. Mennucci, G. A. Petersson, H. Nakatsuji, M. Caricato, X. Li, H. P. Hratchian, A. F. Izmaylov, J. Bloino, G. Zheng, J. L. Sonnenberg, M. Hada, M. Ehara, K. Toyota, R. Fukuda, J. Hasegawa, M. Ishida, T. Nakajima, Y. Honda, O. Kitao, H. Nakai, T. Vreven, J. A. Montgomery Jr, J. E. Peralta, F. Ogliaro, M. Bearpark, J. J. Heyd, E. Brothers, K. N. Kudin, V. N. Staroverov, T. Keith, R. Kobayashi, J. Normand, K. Raghavachari, A. Rendell, J. C. Burant, S. S. Iyengar, J. Tomasi, M. Cossi, N. Rega, J. M. Millam, M. Klene, J. E. Knox, J. B. Cross, V. Bakken, C. Adamo, J. Jaramillo, R. Gomperts, R. E. Stratmann, O. Yazyev, A. J. Austin, R. Cammi, C. Pomelli, J. W. Ochterski, R. L. Martin, K. Morokuma, V. G. Zakrzewski, G. A. Voth, P. Salvador, J. J. Dannenberg, S. Dapprich, A. D. Daniels, O. Farkas, J. B. Foresman, J. V. Ortiz, J. Cioslowski and D. J. Fox, *Gaussian 09, Revision D.01*, Gaussian, Inc., Wallingford CT, 2013.
46 J.-D. Chai and M. Head-Gordon, *Phys. Chem. Chem. Phys.*, 2008, **10**, 6615–6620.
47 A. Austin, G. A. Petersson, M. J. Frisch, F. J. Dobek, G. Scalmani and K. Throssell, *J. Chem. Theory Comput.*, 2012, **8**, 4989–5007.
48 M. M. Francl, W. J. Pietro, W. J. Hehre, J. S. Binkley, M. S. Gordon, D. J. DeFrees and J. A. Pople, *J. Chem. Phys.*, 1982, **77**, 3654–3665.